



G.G. Rooney^{1,2},†

¹Met Office, FitzRoy Road, Exeter EX1 3PB, UK

(Received 15 November 2021; revised 29 April 2022; accepted 31 May 2022)

Dynamical constraints on the wall layer in turbulent pipe flow imply both a narrow peak in the streamwise component of the turbulent Lamb vector near the wall, and a scaling of the wall layer depth proportional to the depth of the viscous sublayer. An approximation of the Lamb vector distribution, which equates to the gradient of Reynolds stress, is proposed. Hence the equation for streamwise mean flow may be integrated to obtain an expression for the velocity profile in the wall layer.

Key words: boundary layer, pipe flow

1. Introduction

Turbulent flow in cylindrical pipes is of great practical and theoretical interest. The transition to turbulence in pipe flow is also a paradigm of turbulent transition, of interest in its own right. The response of fluid flux to an applied pressure gradient depends on the stress at the pipe wall and its transmission to the bulk flow, which is governed by the turbulence structure of the wall layer. Better understanding of this aids the design of efficient flow systems. Flow in this region is usually modelled based on similarity theory, and decomposed into a viscous sublayer and a log layer with experimentally determined coefficients (e.g. Hinze 1959; Townsend 1976).

Here, some dynamical constraints on the wall layer are discussed. These allow an approximate form of the gradient of Reynolds stress there to be postulated, as well as the wall-layer thickness. Thus a mean wall-layer velocity profile may be derived, which compares well with results from previous experimentation.

2. Steady, axisymmetric pipe flow

2.1. Reynolds-averaged mean flow equation

The flow in a smooth pipe of radius R is represented in cylindrical polar coordinates r, ϕ , z as an axisymmetric mean flow in the z direction, varying with radius r and with unsteady

† Email address for correspondence: gabriel.rooney@metoffice.gov.uk

²School of Mathematics, University of Leeds, Leeds LS2 9JT, UK

fluctuations of velocity u':

$$\mathbf{u} = U(r)\hat{\mathbf{z}} + \mathbf{u}',\tag{2.1a}$$

$$\mathbf{u'} = u'\hat{\mathbf{z}} + v'\hat{\boldsymbol{\phi}} + w'\hat{\mathbf{r}}.\tag{2.1b}$$

The mean pressure is denoted P. It is a common observation or assumption that for steady, fully developed pipe flow, dP/dz is approximately constant.

The z-component of the Reynolds-averaged momentum equation for mean flow in a smooth pipe is (Townsend 1976, § 5.2)

$$\frac{1}{r}\frac{\partial}{\partial r}(r\overline{u'w'}) = -\frac{1}{\rho}\frac{\partial P}{\partial z} + \frac{v}{r}\frac{\partial}{\partial r}\left(r\frac{\partial U}{\partial r}\right),\tag{2.2}$$

where ρ and ν are the fluid density and kinematic viscosity, respectively. Inasmuch as it contains fewer terms, this is less complex than the turbulent kinetic energy (TKE) equation. Outside the wall layer, the last term in (2.2) becomes insignificant.

The viscous and Reynolds stresses may be combined into a total stress

$$\tau = \nu \frac{\partial U}{\partial r} - \overline{u'w'} \tag{2.3}$$

which tends to zero at the axis r = 0 and has a value τ_o at r = R. This wall value is a viscous contribution (e.g. Wu & Moin (2008), figure 22), since both limits of the Reynolds stress tend to zero.

The external parameters which characterise flow in a smooth pipe may be taken as the pipe radius R, the pressure gradient along the pipe per unit fluid density,

$$H = -\frac{1}{\rho} \frac{\mathrm{d}P}{\mathrm{d}z} > 0 \tag{2.4}$$

and the kinematic viscosity. Of these, R and H are appropriate for non-dimensionalising turbulent flow, and hereafter a hat $(\hat{\cdot})$ denotes the dimensionless equivalent of a previously dimensional quantity, e.g.

$$\hat{U} = \frac{U}{R^{1/2}H^{1/2}}. (2.5)$$

2.2. The friction factor and Prandtl's formula

The dimensionless friction factor, f, is defined in terms of the pressure gradient, pipe diameter and dynamic pressure of the mean flow speed \mathcal{U} (defined as the volume flux per unit area) as follows:

$$f = \left| \frac{\mathrm{d}P}{\mathrm{d}z} \right| \frac{2R}{\frac{1}{2}\rho \mathcal{U}^2} = \frac{4}{\hat{\mathcal{U}}^2}.$$
 (2.6)

The Reynolds number is

$$Re = \frac{(2R)\mathcal{U}}{\mathcal{V}} = 2\hat{\mathcal{U}}M,\tag{2.7}$$

where

$$M = \frac{R^{3/2}H^{1/2}}{\nu}. (2.8)$$

Turbulent boundary layers are often modelled in terms of the friction velocity $u_* = (\tau_1/\rho)^{1/2}$, where $\tau_1 \sim \tau_0$ is the peak Reynolds stress beyond the wall layer. Assuming that

the viscous term is very small over almost the entire radial range, i.e. neglecting a thin layer at the pipe wall, (2.2) may be integrated to give

$$u_*^2 \approx \frac{HR}{2}.\tag{2.9}$$

The surface-layer similarity assumption $dU/dy \propto u_*/y$ (von Kármán 1931) leads to the log profile

$$\frac{U}{u_*} = k^{-1} \ln \frac{y}{y_1},\tag{2.10}$$

where y is the direction normal to the boundary surface at y = 0, $k \approx 0.4$ is von Kármán's constant, and the integration constant becomes a length scale y_1 to be determined. For pipe flow, y = R - r and, in smooth pipes, y_1 is taken to be the length scale v/u_* of the viscous layer. From (2.9), the dimensionless viscous length scale behaves as

$$\frac{v}{Ru_*} \approx \frac{\sqrt{2}}{M}.\tag{2.11}$$

Combination and experimental calibration of the above relations leads to Prandtl's formula for flow in smooth pipes (Prandtl 1933),

$$f^{-1/2} = -2.0\log_{10}\left(\frac{2.51}{f^{1/2}Re}\right). \tag{2.12}$$

Wall-layer data are often presented as velocities scaled by u_* as a function of distance in wall units, that is, distance scaled by v/u_* . This scaling is denoted by a superscript +. Then (2.11) gives the approximate equivalences,

$$y^{+} = \frac{yu_{*}}{v} = \frac{M}{\sqrt{2}}\hat{y},\tag{2.13a}$$

$$U^{+} = \frac{U}{u_{*}} = \sqrt{2}\hat{U}. \tag{2.13b}$$

The viscous sublayer is conventionally specified as extending through $0 \le y^+ \le 5$, while the wall layer extends to $y^+ \approx 30$. In the viscous layer very close to the wall it is expected that (e.g. Townsend (1976), § 5.9)

$$U^{+} \approx y^{+}. \tag{2.14}$$

3. The turbulent Lamb vector

3.1. Relationship to Reynolds stress

The Reynolds stress gradient may be identified with the z-component of the turbulent Lamb vector $\ell'' = \omega' \times u'$,

$$\overline{\ell_z''} = \frac{1}{r} \frac{\partial}{\partial r} (r \, \overline{u'w'}),\tag{3.1}$$

where $\omega' = \nabla \times u'$ is the turbulent vorticity (see Appendix A). This is significant because the turbulent velocity fluctuations tend to zero at the pipe wall, hence so do the components of ℓ'' . (The azimuthal component of ℓ'' may be assumed negligible throughout, while the radial component is in a three-way balance with the radial gradients of mean pressure and TKE.)

Equation (2.2) may then be written in dimensionless form as

$$\frac{1}{\hat{r}}\frac{\partial}{\partial \hat{r}}\left(\hat{r}\frac{\partial \hat{U}}{\partial \hat{r}}\right) = M(\mathcal{L} - 1),\tag{3.2}$$

where the dimensionless *z*-component of the Lamb vector is denoted by $\mathcal{L} (= \overline{\ell''_{\tau}}/H)$.

3.2. Behaviour in the different layers

At intermediate Re (\sim 10⁴), the turbulent stress is observed as linearly increasing with radius in the bulk of the flow, before decreasing rapidly in the wall layer. This is consistent with a first-order balance between the turbulent stress and the pressure gradient in the main part of the flow.

Thus in the core, simply omitting the shear-dependent term from (3.2),

$$\mathcal{L} \approx 1$$
 (3.3)

which agrees with the observed linear radial dependence of $\overline{u'w'}$ in this region.

The thickness of the wall layer is denoted d, so that the core extends through 0 < r < R - d and the wall layer through R - d < r < R. In the wall layer, the assumption of a steady, z-invariant mean state implies that the pressure gradient should equal that in the core, or else a radial pressure gradient would appear at downstream locations (Hinze 1959, § 7.8). The boundary conditions may be specified as

$$\begin{aligned}
\hat{U} &= 0, & \mathcal{L} &= 0 & \text{at } \hat{r} &= 1 \\
\frac{\partial \hat{U}}{\partial \hat{r}} &= G, & \mathcal{L} &= 1 & \text{at } \hat{r} &= 1 - \hat{d}
\end{aligned} \tag{3.4}$$

where G is the velocity gradient at the inner edge of the wall layer, as yet unknown.

3.3. Model of the Lamb-vector component in the wall layer

Since $\overline{u'w'} \to 0$ as $r \to R$, (3.1) implies that

$$\int_0^R r \, \overline{\ell_z''} \, \mathrm{d}r = 0. \tag{3.5}$$

From this constraint, and the very simple core-region approximation (3.3), it would then seem that $\overline{\ell_z''}$ must have a radial distribution like that sketched in figure 1. Thus, from (3.3),

$$\int_0^{R-d} r \,\overline{\ell_z''} \,\mathrm{d}r \approx \frac{1}{2} (R-d)^2 H \tag{3.6}$$

and hence

$$\int_{R-d}^{R} r \,\overline{\ell_z''} \,\mathrm{d}r \approx -\frac{1}{2} (R-d)^2 H. \tag{3.7}$$

That is, $\overline{\ell_z''}$ must have substantial negative values in the wall layer since $d \ll R$.

Examples of the profiles of Reynolds stress and the turbulent Lamb-vector component are shown in figure 2. These are based on the data of Wu & Moin (2008), obtained from https://ctr.stanford.edu/research-data.

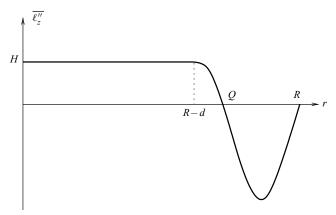


Figure 1. Sketch of the radial profile of $\overline{\ell_z''}$, given the constraints of constancy in the core region r < R - d and null values of $\overline{\ell_z''}$ and Reynolds stress at r = R. The profile intersects the r axis at Q and R.

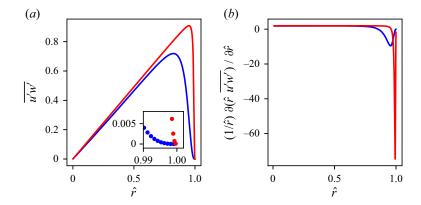


Figure 2. Example profiles of (a) the Reynolds stress, and (b) the streamwise component of the turbulent Lamb vector, at Re = 5300 (blue) and $Re = 44\,000$ (red). These are based on the data of Wu & Moin (2008). The inset to (a) shows individual data points, indicating the extent to which the simulations resolve the fine structure near the wall. The Lamb-vector component has been calculated from the Reynolds stress using (3.1).

Considering for instance the contribution to $\overline{\ell_z''}$ from the combination of azimuthal vorticity and radial velocity fluctuations (possibly the dominant contribution in pipe geometry), the implications of this for the flow structure are that a strong helical correlation in one azimuthal direction in the wall layer has a weaker counterpart in the other direction in the core of the flow. It may be speculated that the vortex generation and flow inflections at the laminar–turbulent transition observed by Hof *et al.* (2010) are related to the establishment of turbulent structures of this sort.

To facilitate an initial, simplified analysis, the profile of $\overline{\ell_z''}$ in the wall layer may be approximated by a parabola

$$\overline{\ell_z''} = A(r - R)(r - Q), \tag{3.8}$$

where $R - d \le Q \le R$. The values of A and Q are determined by H and d as follows. At r = R - d, continuity of $\overline{\ell_z''}$ implies

$$Ad(d-q) = H, (3.9)$$

where q = R - Q. Also

$$\int_{R-d}^{R} r \, \overline{\ell_z''} \, dr = A \int_{R-d}^{R} r(r-R)(r-Q) \, dr$$

$$= -Ad^2 \left(\frac{1}{4} d^2 - \frac{R+q}{3} d + \frac{Rq}{2} \right)$$
(3.10)

so that, from (3.7),

$$Ad^{2}\left(\frac{1}{4}d^{2} - \frac{R+q}{3}d + \frac{Rq}{2}\right) = \frac{1}{2}(R-d)^{2}H.$$
 (3.11)

Hence from (3.9)

$$q = d \left(\frac{3\hat{d}^2 - 8\hat{d} + 6}{2\hat{d}^2 - 6\hat{d} + 6} \right) \quad \Rightarrow \quad d - q = d \left(\frac{2\hat{d} - \hat{d}^2}{2\hat{d}^2 - 6\hat{d} + 6} \right) \tag{3.12}$$

and so

$$Q = R\left(\frac{-3\hat{d}^3 + 10\hat{d}^2 - 12\hat{d} + 6}{2\hat{d}^2 - 6\hat{d} + 6}\right)$$
(3.13)

so that

$$\hat{Q} \to 1 - \hat{d} \quad \text{as } \hat{d} \to 0.$$
 (3.14)

Using (3.9), (3.8) may be written

$$\overline{\ell_z''} = \frac{H}{d(d-q)}(r-R)(r-Q)$$
 (3.15)

or

$$\mathcal{L} = B(\hat{r} - 1)(\hat{r} - \hat{Q})$$

$$= B(\hat{r}^2 - (1 + \hat{Q})\hat{r} + \hat{Q})$$
(3.16)

where \hat{Q} is given by (3.13), and

$$B = \frac{1}{\hat{d}(\hat{d} - \hat{q})} \tag{3.17}$$

so that, from (3.12),

$$B \to \frac{3}{\hat{d}^3} \quad \text{as } \hat{d} \to 0.$$
 (3.18)

An example of the function (3.15) is shown in figure 3, along with the corresponding integrand $r \overline{\ell_z''}$.

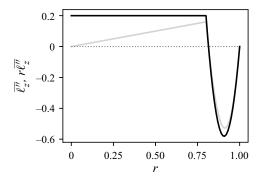


Figure 3. Example plots of the present approximation to $\overline{\ell_z''}$ (black solid), and hence $r \overline{\ell_z''}$ (grey solid), taking R = 1, H = 0.2 and d = 0.2. The model (3.15) is plotted in region r > (R - d), and (3.3) elsewhere.

4. Mean velocity profile in the wall layer

4.1. Form of the velocity profile

Using (3.16) and the boundary conditions (3.4), (3.2) may be integrated to give

$$\frac{\hat{U}}{M} = \frac{1}{16}B(\hat{r}^4 - 1) - \frac{1}{9}B(1 + \hat{Q})(\hat{r}^3 - 1) + \frac{1}{4}(B\hat{Q} - 1)(\hat{r}^2 - 1)
- \left(\frac{1}{4}B(1 - \hat{d})^4 - \frac{1}{3}B(1 + \hat{Q})(1 - \hat{d})^3 + \frac{1}{2}(B\hat{Q} - 1)(1 - \hat{d})^2\right)\ln\hat{r}
+ (1 - \hat{d})\left(\frac{\hat{G}}{M}\right)\ln\hat{r}.$$
(4.1)

The maximum value of \hat{U} in this layer, denoted \hat{U}_L , will be at $\hat{r} = 1 - \hat{d}$, and is given by

$$\frac{\hat{U}_L}{M} - (1 - \hat{d}) \left(\frac{\hat{G}}{M}\right) \ln(1 - \hat{d}) = \frac{1}{16} B \left((1 - \hat{d})^4 \left[1 - 4 \ln(1 - \hat{d}) \right] - 1 \right)
- \frac{1}{9} B (1 + \hat{Q}) \left((1 - \hat{d})^3 \left[1 - 3 \ln(1 - \hat{d}) \right] - 1 \right)
+ \frac{1}{4} (B \hat{Q} - 1) \left((1 - \hat{d})^2 \left[1 - 2 \ln(1 - \hat{d}) \right] - 1 \right).$$
(4.2)

To gauge the behaviour at small \hat{d} , the terms on the right-hand side of (4.2) may be expanded up to \hat{d}^4 , see Appendix B, which is necessary given the limiting behaviour of B (3.18). (Cancellation of terms means that the approximation (3.14) is sufficient for \hat{Q} .) For the terms on the left-hand side of (4.2) it is assumed, and verified later, that $M \gg 1$ as $\hat{d} \ll 1$ so that only $O(M^{-1})$ terms should be retained at the end.

Regarding G, observations suggest that, at intermediate Re, there is relatively little shear in the core of the flow compared with the layer at the wall, so that the velocity in the core is comparable to that at the edge of the wall layer. This suggests an approximate scaling of

$$\hat{G} \approx -\frac{\hat{U}_L}{1 - \hat{d}}.\tag{4.3}$$

Hence, for small \hat{d} ,

$$\frac{\hat{U}_L}{M} \left(1 + \ln(1 - \hat{d}) \right) \approx \frac{\hat{d}^2}{2} + \left(2B\hat{d} - 1 \right) \frac{\hat{d}^3}{6} + \left(-6B - 3B\hat{d} - 1 \right) \frac{\hat{d}^4}{24}. \tag{4.4}$$

Then substituting for B from (3.18) and retaining only the leading-order terms on each side,

$$\frac{\hat{U}_L}{M} \approx \frac{\hat{d}}{4} \quad \text{as } \hat{d} \to 0.$$
 (4.5)

The relationships (4.3) and (4.5) may be combined to substitute for G,

$$(1 - \hat{d})\frac{\hat{G}}{M} \approx -\frac{\hat{d}}{4} \tag{4.6}$$

so that (4.1) becomes

$$\frac{\hat{U}}{M} = \frac{1}{16}B(\hat{r}^4 - 1) - \frac{1}{9}B(1 + \hat{Q})(\hat{r}^3 - 1) + \frac{1}{4}(B\hat{Q} - 1)(\hat{r}^2 - 1)
- \left(\frac{1}{4}B(1 - \hat{d})^4 - \frac{1}{3}B(1 + \hat{Q})(1 - \hat{d})^3 + \frac{1}{2}(B\hat{Q} - 1)(1 - \hat{d})^2\right)\ln\hat{r} - \frac{\hat{d}}{4}\ln\hat{r}.$$
(4.7)

4.2. Scaling of the layer depth

The above analysis yields a hypothetical velocity profile in the wall layer as a function of its depth \hat{d} . It does not predict \hat{d} . To further interpret the velocity profile, the scaling of \hat{d} must be considered, and one relevant aspect is the Reynolds number of the wall layer.

The Reynolds number is often defined simply in terms of length and velocity scales. However, there is also an implicit assumption about flow structure, namely that the velocity should vary by the order of the velocity scale, over a distance given by the length scale. Otherwise, the definition would not be Galilean-invariant, for instance.

To retain the mean-velocity term in the momentum equation (3.2), which is present due to the viscosity being non-negligible, there is an implication that the Reynolds number of the wall layer should be bounded. This is a further constraint on the system. Denoting this shear-layer Reynolds number by \mathcal{R} , it is defined as

$$\mathcal{R} = \frac{U_L d}{v} = M \hat{U}_L \hat{d}. \tag{4.8}$$

The continued existence of the shear layer may imply that \mathcal{R} approaches some limiting value, \mathcal{R}_c . Then the asymptotic behaviour of (4.5) becomes $\hat{U}_L/M \approx \mathcal{R}_c/(4M\hat{U}_L)$, so that

$$\hat{U}_L \approx \frac{\mathcal{R}_c^{1/2}}{2} \tag{4.9}$$

and then from (4.8)

$$\hat{d} \approx \frac{2\mathcal{R}_c^{1/2}}{M}.\tag{4.10}$$

This is the same M-dependence as (2.11), which implies that \hat{d} is simply as a multiple of the viscous length scale, as might be expected.

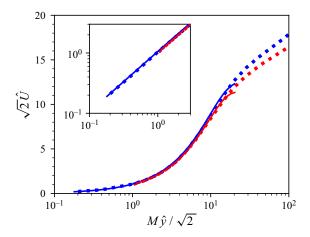


Figure 4. Mean flow speed in the wall layer. The solid lines show predictions for Re = 5300 (blue) and Re = 44000 (red) using equation (4.7) over the range $10^{-3} < \hat{y} < \hat{d}$. The dashed lines show loci of data from Wu & Moin (2008) at the same values of Re, also in blue and red, respectively. The inset shows the same data at low values of \hat{y} , with both axes logarithmic.

4.3. Comparison with data

To compare the present model with previous studies, it is simplest to make use of Prandtl's formula to relate M to Re. Thus, a choice of Re gives the expected corresponding value for f from (2.12), which then defines $M = Ref^{1/2}/4$, and hence \hat{d} from a chosen value of \mathcal{R}_c . The wall-layer profile (4.7) may then be compared with previous data.

Figure 4 shows data from Wu & Moin (2008) (see their figures 1 and 9) at Re = 5300 and $Re = 44\,000$ (dashed lines), and (4.7) for the same values of Re (solid lines) taking the shear-layer limiting value as $\mathcal{R}_c = 250$. These correspond to M values of 2.5×10^2 , 1.6×10^3 and \hat{d} values of 1.2×10^{-1} , 2.0×10^{-2} , respectively, so that $M\hat{d} \approx 32$. The chosen value of \mathcal{R}_c thus implies a depth of the wall layer of approximately 23 wall units, i.e. $M\hat{d}/\sqrt{2} \approx 23$, see (2.13). This is smaller, though of comparable magnitude to the usual estimate of around 30 wall units.

With this value of \mathcal{R}_c , it can be seen that (4.7) matches closely to the data over a large part of the wall-layer range, although there is a deviation from the data at the inner end of the wall layer (noting that the ordinate of the main plot in figure 4 is linear).

It may be expected that a more sophisticated model of \mathcal{L} and/or G could improve the model here. Smoothing the transition from the wall layer to the core may also improve the small underestimate of the wall-layer depth.

At the greater Re value, the maximum speed from this model corresponds closely to the approximation (4.5).

5. Conclusion

Dynamical constraints on the wall layer in turbulent pipe flow have been discussed. These imply both a narrow peak in the streamwise component of the turbulent Lamb vector near the wall, and a scaling of the wall-layer depth proportional to the depth of the viscous sublayer. Fitting an approximate form to the Lamb-vector component allows integration of the equation for streamwise mean flow, resulting in an expression for the whole wall-layer mean velocity profile which compares satisfactorily with previous data.

The wall-layer velocity profile bridges the gap between the no-slip pipe wall and the velocity scale of the flow in the core. Understanding its structure contributes to validation of flow modelling by numerical or experimental methods. It also aids the extrapolation and generalisation of experimental results obtained in specific cases.

The approximation to the Lamb-vector profile is applied over the entire wall layer. This approach contrasts with that of Klewicki (2021) for instance, who compares the force balance in various sublayers in a turbulent channel, and also suggests there may be some different effects due to the cylindrical geometry of a pipe. The use of the Lamb vector herein emphasises the apparent constraint that the geometry imposes on the wall layer in relation to the core flow (consider, for instance, the radial integrand plotted in figure 3). In addition, the explicit dependence of the Lamb vector on turbulent vorticity suggests an interpretation of turbulent pipe flow in terms of azimuthal vortex structures. Corrsin (1961) described turbulence as 'a random field of vorticity', emphasising the need to consider vorticity fluctuations as well as velocity fluctuations. See Hamman, Klewicki & Kirby (2008) for further discussion of the Lamb vector in a variety of contexts, including turbulent channel flow.

The model developed is based on typical engineering assumptions of a constant pressure gradient and a steady mean state, as in the standard treatment of laminar flow. Thus far it requires no information on the details of the turbulent structures in the wall layer. However, incorporation of such information may be helpful in developing it further.

Acknowledgements. G.G.R. gratefully acknowledges the support of the Cheney Fellowship scheme at the University of Leeds.

Declaration of interests. The author reports no conflict of interest.

Author ORCIDs.

G.G. Rooney https://orcid.org/0000-0002-3787-1198.

Appendix A. The streamwise Lamb vector in cylindrical polar coordinates

In cylindrical polar coordinates the continuity equation is

$$\nabla \cdot \boldsymbol{u} = \frac{1}{r} \frac{\partial}{\partial r} (r\boldsymbol{u}) + \frac{1}{r} \frac{\partial \boldsymbol{v}}{\partial \phi} + \frac{\partial \boldsymbol{w}}{\partial z} = 0 \tag{A1}$$

and the vorticity is

$$\boldsymbol{\omega} = \left(\frac{1}{r}\frac{\partial w}{\partial \phi} - \frac{\partial v}{\partial z}\right)\hat{\boldsymbol{r}} + \left(\frac{\partial u}{\partial z} - \frac{\partial w}{\partial r}\right)\hat{\boldsymbol{\phi}} + \frac{1}{r}\left(\frac{\partial}{\partial r}(rv) - \frac{\partial u}{\partial \phi}\right)\hat{\boldsymbol{z}}.\tag{A2}$$

The z-component of the Lamb vector is

$$\ell_z = \omega_r v - \omega_\phi u = \left(\frac{1}{r} \frac{\partial w}{\partial \phi} - \frac{\partial v}{\partial z}\right) v - \left(\frac{\partial u}{\partial z} - \frac{\partial w}{\partial r}\right) u \tag{A3}$$

and with the addition of $w\nabla \cdot u$ (=0) this becomes

$$\ell_z = \frac{1}{r} \frac{\partial}{\partial r} (ruw) + \frac{1}{r} \frac{\partial}{\partial \phi} (vw) + \frac{\partial}{\partial z} (w^2) - \frac{1}{2} \frac{\partial}{\partial z} (u^2 + v^2 + w^2)$$
 (A4)

so that

$$\ell_z + \frac{1}{2} \frac{\partial}{\partial z} (\boldsymbol{u} \cdot \boldsymbol{u}) = \frac{1}{r} \frac{\partial}{\partial r} (ruw) + \frac{1}{r} \frac{\partial}{\partial \phi} (vw) + \frac{\partial}{\partial z} (w^2)$$

$$= \nabla \cdot (w\boldsymbol{u}) \tag{A5}$$

as expected.

The same result may be obtained when considering turbulent fluctuations only, in which case it relates the *z*-component of the turbulent Lamb vector to the TKE and Reynolds stresses in the usual manner (e.g. Tennekes & Lumley (1972), their (3.3.13)). For steady turbulent pipe flow, downstream and azimuthal gradients may be neglected, and hence

$$\overline{\ell_z''} = \frac{1}{r} \frac{\partial}{\partial r} (r \overline{u'w'}). \tag{A6}$$

Thus $\overline{\ell_z''}$ effectively represents that part of the Reynolds-stress gradient which remains significant, i.e. formally removing the TKE gradient.

Appendix B. Expansions

For $0 < x \ll 1$,

$$(1-x)^4 \left[1 - 4\ln(1-x)\right] \approx (1 - 4x + 6x^2 - 4x^3 + x^4) \left(1 + 4x + 2x^2 + \frac{4}{3}x^3 + x^4\right)$$

$$\approx 1 - \frac{16}{2}x^2 + \frac{40}{3}x^3 - \frac{22}{3}x^4,$$
(B1)
$$(1-x)^3 \left[1 - 3\ln(1-x)\right] \approx (1 - 3x + 3x^2 - x^3) \left(1 + 3x + \frac{3}{2}x^2 + x^3 + \frac{3}{4}x^4\right)$$

$$\approx 1 - \frac{9}{2}x^2 + \frac{9}{2}x^3 - \frac{3}{4}x^4,$$
(B2)
$$(1-x)^2 \left[1 - 2\ln(1-x)\right] \approx (1 - 2x + x^2) \left(1 + 2x + x^2 + \frac{2}{3}x^3 + \frac{1}{2}x^4\right)$$

$$\approx 1 - \frac{4}{2}x^2 + \frac{2}{3}x^3 + \frac{1}{6}x^4.$$
(B3)

Using the above relations to substitute for each term on the right-hand side of (4.2) gives, for small \hat{d} ,

$$\frac{\hat{U}_L}{M} - (1 - \hat{d}) \left(\frac{\hat{G}}{M}\right) \ln(1 - \hat{d}) \approx \frac{1}{16} B \left(-\frac{16}{2} \hat{d}^2 + \frac{40}{3} \hat{d}^3 - \frac{22}{3} \hat{d}^4\right) \\
- \frac{1}{9} B (1 + \hat{Q}) \left(-\frac{9}{2} \hat{d}^2 + \frac{9}{2} \hat{d}^3 - \frac{3}{4} \hat{d}^4\right) \\
+ \frac{1}{4} (B \hat{Q} - 1) \left(-\frac{4}{2} \hat{d}^2 + \frac{2}{3} \hat{d}^3 + \frac{1}{6} \hat{d}^4\right) \\
= \left(-B + B (1 + \hat{Q}) - (B \hat{Q} - 1)\right) \frac{\hat{d}^2}{2} \\
+ \left(5B - 3B (1 + \hat{Q}) + (B \hat{Q} - 1)\right) \frac{\hat{d}^3}{6} \\
+ \left(-11B + 2B (1 + \hat{Q}) + (B \hat{Q} - 1)\right) \frac{\hat{d}^4}{24} \\
= \frac{\hat{d}^2}{2} + \left(5B - 3B (1 + \hat{Q}) + (B \hat{Q} - 1)\right) \frac{\hat{d}^3}{6} \\
+ \left(-11B + 2B (1 + \hat{Q}) + (B \hat{Q} - 1)\right) \frac{\hat{d}^4}{24}. \tag{B4}$$

G.G. Rooney

The lack of O(x) terms in (B1)–(B3), plus a cancellation of \hat{Q} terms at $O(\hat{d}^2)$, means that the approximation (3.14) is sufficient for \hat{Q} . Hence

$$\frac{\hat{U}_L}{M} - (1 - \hat{d}) \left(\frac{\hat{G}}{M}\right) \ln(1 - \hat{d}) \approx \frac{\hat{d}^2}{2} + \left(5B - 3B(2 - \hat{d}) + (B(1 - \hat{d}) - 1)\right) \frac{\hat{d}^3}{6} + \left(-11B + 2B(2 - \hat{d}) + (B(1 - \hat{d}) - 1)\right) \frac{\hat{d}^4}{24} \\
\approx \frac{\hat{d}^2}{2} + \left(2B\hat{d} - 1\right) \frac{\hat{d}^3}{6} + \left(-6B - 3B\hat{d} - 1\right) \frac{\hat{d}^4}{24}. \quad (B5)$$

REFERENCES

CORRSIN, S. 1961 Turbulent flow. Am. Sci. 49 (3), 300-325.

HAMMAN, C.W., KLEWICKI, J.C. & KIRBY, R.M. 2008 On the Lamb vector divergence in Navier–Stokes flows. *J. Fluid Mech.* **610**, 261–284.

HINZE, J.O. 1959 Turbulence. McGraw-Hill.

HOF, B., DE LOZAR, A., AVILA, M., TU, X. & SCHNEIDER, T.M. 2010 Eliminating turbulence in spatially intermittent flows. *Science* **327** (5972), 1491–1494.

VON KÁRMÁN, T. 1931 Mechanical similitude and turbulence. NACA Tech. Rep. NACA-TM-611. National Advisory Committee for Aeronautics, USA, English translation from Nachrichten von der Gesellschaft der Wissenschaften zu Göttingen, 1930.

KLEWICKI, J.C. 2021 Properties of turbulent channel flow similarity solutions. J. Fluid Mech. 915, A39.

PRANDTL, L. 1933 Recent results of turbulence research. NACA Tech. Rep. NACA-TM-720. National Advisory Committee for Aeronautics, USA, English translation from Zeitschrift des Vereines Deutscher Ingenieure, 1933.

TENNEKES, H. & LUMLEY, J.L. 1972 A First Course in Turbulence. MIT.

TOWNSEND, A.A. 1976 The Structure of Turbulent Shear Flow. Cambridge University Press.

WU, X. & MOIN, P. 2008 A direct numerical simulation study on the mean velocity characteristics in turbulent pipe flow. *J. Fluid Mech.* **608**, 81–112 (Data are available from https://ctr.stanford.edu/research-data).